

# The Energy of High Frequency Waves in the Low Solar Chromosphere

A. Anđić<sup>1,2</sup>

<sup>1</sup> *Astronomical Research Centre, Queen's University Belfast, University Road, Belfast, BT7 1NN, UK (a.andic@qub.ac.uk)*

<sup>2</sup> *Institut für Astrophysik, Friedrich-Hund-Platz 1, 37077 Göttingen, Germany*

Received: date

**Abstract.** High frequency acoustic waves have been suggested as a source of mechanical heating in the chromosphere. In this work the radial component of waves in the frequency interval 22mHz to 1mHz are investigated. Observations were performed using 2D spectroscopy in the spectral lines of Fe I 543.45nm and Fe I 543.29nm at the Vacuum Tower Telescope, Tenerife, Spain. Speckle reconstruction has been applied to the observations. We have used Fourier and wavelet techniques to identify oscillatory power. The energy flux is estimated assuming that all observed oscillations are acoustics running waves. We find that the estimated energy flux is not sufficient to cover the chromospheric radiative losses.

**Keywords:** Sun: chromosphere, Sun: oscillations, Sun: heating

## 1. Introduction

The temperature of the Solar atmosphere first decreases with height, reaching a minimum at approximately 500km<sup>1</sup> and then increases until it reaches coronal values (Vernazza, Avret and Loeser, 1981). During the last century, high frequency acoustic waves were suggested as a source of mechanical heating. Their origin was believed to be below the photosphere. Propagating upwards through the solar atmosphere, they form shocks and dissipate energy in the chromosphere. Ulmschneider (1971a, 1971b, 2003) suggested that waves with frequencies from 6mHz to 100mHz are the main carrier of the required energy and the peak energy transport should occur with waves of frequencies above 20mHz.

An important question of the chromospheric heating problem is whether mechanical heating is sufficient to balance radiative losses (*e.g.*, Kalkofen, 2001). The energy required to balance the radiative losses just above the temperature minimum is around  $14 \times 10^3 \text{ Wm}^{-2}$  (Anderson and Athay, 1989). The existence of the chromosphere depends on a constant energy supply, in time, provided by mechanical heating (Ulmschneider, 2003).

The generation of acoustic waves can be described by the ‘Lighthill mechanism’ (Lighthill, 1951). Acoustic waves appear to be generated by tur-

---

<sup>1</sup> where the region with  $\tau_{500} = 1$  is taken as the reference point.

bulence eddies for which the dissipation of kinetic energy by viscosity is negligible (Proudman, 1952). The majority of acoustic waves originate from isolated sources which occupy relatively small volumes, but the nature of those sources is not clear (Deubner and Laufer, 1983). The most energetic oscillations should be generated in those regions where the convective velocities are largest. The energy carried by the waves is sensitive to the Mach number of the turbulence and to the frequency of the emitted waves (Stein, 1967).

High frequency acoustic waves will form shocks within a few scale heights; low frequency waves need larger scales to shock (Stein and Leibacher, 1974). Heating by dissipation of acoustic shocks is time dependent (Carlsson and Stein, 1995).

During wave propagation through the solar atmosphere their velocity amplitude increases with decreasing density, which will cause a height-dependent variation of their frequency. These changes are caused by the resonance absorption, the merging of shocks, and from shocks ‘cannibalizing’ each other (Ulmschneider, 2003). Cram, Keil and Ulmschneider (1979) and Durrant (1980) recommend the use of the observed velocity fields and the analysis of the micro turbulent velocities caused by high frequency acoustic waves.

Several observations detected high frequency waves (Liu, 1974; Mein and Mein, 1976; von Uexküll *et al.*, 1985; Hansteen, Betta and Carlsson, 2000; Wunnenberg, Andjic and Kneer, 2003). The observed energy has been discussed by several authors (Liu, 1974; Lites and Chipman, 1979) who concluded that it is too small to cover the chromospheric losses. However, from the theoretical standpoint, there is a possibility that acoustic waves carry enough energy flux to cover the needs of the chromosphere (Ulmschneider, 2003; Kalkofen, 1990, 2001). Wunnenberg, Kneer and Hirzberger (2002) claim that short period acoustic waves have enough energy for heating the chromosphere.

In the recent works of Domínguez (2004), Andjic and Wiehr (2006) and Andic and Voćkić (2007) there is evidence for magnetic activity even in the so called “non- magnetic” internetwork. This would question the assumption that the observed high oscillations are purely acoustic in origin. Based on TRACE observations Fossum and Carlsson (2006) claim there is not enough acoustic energy flux to heat the chromosphere and that magnetic fields in the internetwork are more significant than previously thought.

## 2. Observations

The data sets used in the analysis of this work were obtained using high-cadence observations of the Fe I spectral lines 543.45nm ( $g_L = 0$ ) and 543.29nm ( $g_L = 0.335$ ). The 2D spectroscopy was performed using the

Table I. Information about the data sets used in this work, dates, used lines and object of observation for obtained data sets. The areas marked as ‘Quiet Sun’ are quiet internetwork.

Data set	Lines used	Object of observation	Coordinates	Images	Exposure [ms]	Cadence [s]
DS1	543.45 and 543.29	Quiet Sun	[0, 0]	108	30	28.4
DS2	543.45 and 543.29	Bright points	[0, 0]	108	30	28.4
DS3	543.45	Pore	[0, 0]	91	20	22.7
DS4	543.45	Quiet Sun	[96.7, 90.7]	91	20	22.7

German Vacuum Tower telescope (VTT) on the Canary islands, with the “Göttingen” Fabry-Perot spectrometer (Bendlin, Volkmer and Kneer, 1992). The instrument setup used in this work has been described in detail by Koschinsky, Kneer and Hirzberger (2001). We have not used a polarimeter in this study.

The post focus instrument is made following the demands of speckle reconstruction (Bendlin, Volkmer and Kneer, 1992; Koschinsky, Kneer and Hirzberger, 2001). Therefore it takes simultaneously two types of images, broadband and narrow-band. The broadband images are images of integrated light in the observed spectral line. The narrow band images are scans through the spectral line using the Fabry-Perot spectrometer. For the scanning, a number of positions in the line, a number of images per position and a exposure time were determined at the beginning of each observation taking into account the atmospheric conditions and requirements imposed by speckle reconstruction (Section 3). In atmospheric conditions with good or very good seeing, the cadence was higher, while during average seeing the cadence was lower. For the data sets where only one line was used, the line is scanned using 13 positions across the profile, of which 2 positions were in the continuum. In the data set with the two lines 18 positions were used, 10 for the stronger line (543.45nm) and 8 for the weaker line (543.29nm) and only one position in the continuum.

The data sets were taken during an observing run in June 2004 (Table I). The adaptive optics system was used (Berkefeld, Soltau, von der Lühe, 2003; Soltau *et al.*, 2002).

One of our main objectives was to achieve the highest cadence possible, which allows us to study waves with the highest frequencies. Since the time evolution of high frequency waves was of main interest, reasonably long time sequences were taken. Solar areas, which showed neither G-band structures nor other magnetic activity, were classified as quiet internetwork regions. For active areas, we selected fields of view with the pores and large numbers

of G-band bright points. The coordinates (Table I) represent the position of the field of view, in arc sec, where the reference point is the centre of the Sun.

### 3. Data Reduction and Analysis Methods

The data reduction for the broadband images was done with a program developed by P. Sutterlin following the method of de Boer, Kneer and Nesis (1992) and de Boer and Kneer (1994). The program included the following procedures: subtraction of darks, flat fielding and speckle reconstruction. The program used for the reconstruction of narrow band images was developed by Janssen (2003) and is based on the method developed by Keller and von der Lühe (1992).

The line bisectors were calculated for each line profile in the 2D spectra to obtain more precise Doppler velocities, since the thermal drifts of the spectrometer may cause the first wavelength position to vary in each scanned line profile. The calculation was performed for each pixel in the reconstructed narrow-band images. All images from one scan are correlated, producing a line profile for each spatial position. The line profiles were then interpolated by a cubic ‘spline’ function and the bisectors calculated. Interpolation is necessary since the spectral line is scanned with a small number of positions in order to maximize the cadence. As a reference point for the calculation of Doppler velocities we took a mean Doppler shift from one 2D spectrum and set it to zero. The procedure is repeated for all data sets. The shift of the bisector value for the core of the line with respect to this reference point corresponds to a Doppler shift, since the wavelength distance between the two scanning positions is known.

Velocity maps used in this work are obtained from the bisector level corresponding to the core of the line profile.

The time evolution was studied by converting the velocity maps into data cubes with time as the third axis. These maps have different sizes as a consequence of the reconstruction procedure of the narrow-band images. It is therefore necessary to do an additional correlation and alignment. This procedure can be carried out accurately only for images where clear structures are visible. Therefore it is done from the reconstructed broadband images which were already cut to the same dimensions as the narrow-band images. The parameters obtained in this way were used for the alignment of the velocity measurements.

In order to determine the height levels corresponding to the calculated bisector levels, the formation layer of the line core have to be known. Our estimate for the formation height of the Fe I 543.45 and 543.29 line cores is based on the location of optical depth unity at the central wavelength as

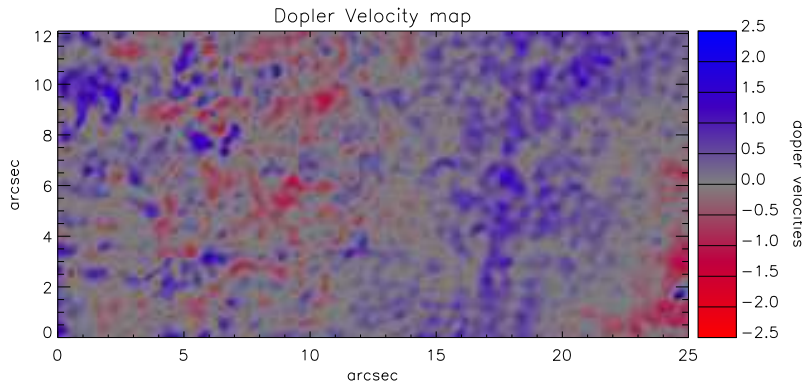


Figure 1. Example of a velocity map at a height of the line core, from the data set DS4.

calculated from a 3-D radiative-hydrodynamic simulation of Asplund *et al.* (2000). An example of the results obtained is shown at the Figure 2. This method is described in detail in the work of Shchukina and Trujillo Bueno (2001).

The average formation heights in LTE, are 308.2km and 660.2km for Fe I 543.29nm and Fe I 543.45nm respectively (N. Shchukina, private correspondence). These formation heights are very close to those obtained with the LTE model of Holweger and Müller (1974).

The solar signal exhibits non-stationarity in both the spatial and temporal domains. Wavelet analysis is, therefore, better suited than Fourier analysis for the interpretation of the observations. For our analysis we chose the Morlet wavelet:

$$\psi_0(t) = \pi^{-\frac{1}{4}} e^{i\omega_0 t} e^{-\frac{t^2}{2}}, \quad (1)$$

where  $\omega_0$  is the non-dimensional frequency and  $t$  the non-dimensional time parameter. This wavelet is non-orthogonal, based on a Gaussian function and sinusoidal wave. The wavelet analysis code used here is based on the work by Torrence and Compo (1998). The associated Fourier period,  $P$ , is 1.03s for  $\omega_0 = 6$ , where  $s$  is the wavelet scale (see Table 1 in Torrence and Compo (1998)). The wavelet transform is a convolution of the time series with the analyzing wavelet, thus a complete wavelet transform is achieved by varying the wavelet scale, which controls both the period and temporal extent of the function and scanning this through the time series. One-dimensional wavelet analysis is done for each spatial coordinate. At the beginning and end of the wavelet transforms there are regions where spurious power may arise as a

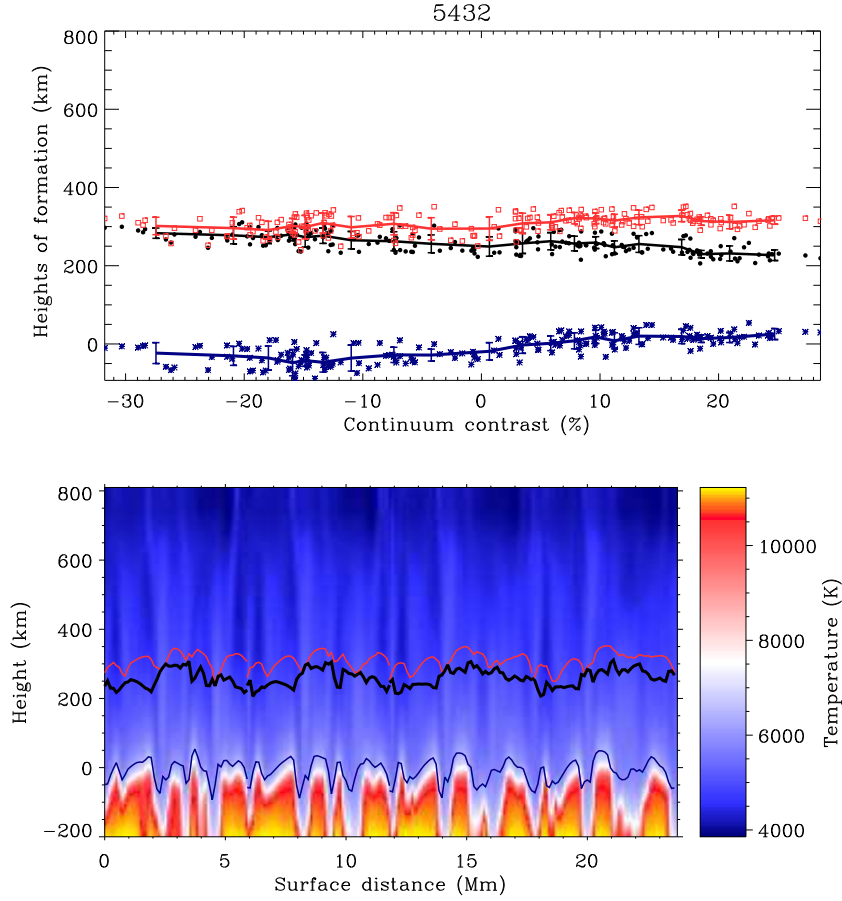


*Figure 2.* Example of a results for the height of the line formation calculated for the spectral line Fe I 453.29nm. The top panel shows the heights vs continuum contrast. The  $y$ -axis gives height of formation in [km]. The LTE case is red color the NLTE is in the black for the line centre. The thin blue line is the height of formation of the line wing *e.g.* continuum. The bottom panel shows the heights vs position along the "solar surface" in Mm. The background shows the vertical temperature of the model. The granules are visible as bright yellow and red features. (With courtesy of the N. Shchukina)

result of the finite extent of the time series. These regions are referred to as the cone of influence (COI), having a temporal extent equal to the  $e$ -folding time ( $t_d$ ) of the wavelet function. In our case it is:

$$t_d = \sqrt{2s} = \sqrt{2} \frac{P}{1.03}. \quad (2)$$

Table II. Values of sound speed and density used for calculations of energy flux.

Height [km]	Speed of sound [m s <sup>-2</sup> ]	Density [kg m <sup>-3</sup> ]
660	6742	$1.32 \times 10^{-6}$
308	7142	$3.46 \times 10^{-5}$

This time scale is the response of the wavelet function to noise spikes and is used in our detection criteria by requiring that reliable oscillations have a duration greater than  $t_d$  outside the COI. This imposed a maximum period of 912s (or  $\approx 1\text{mHz}$ ) above which any detected periods were disregarded. The automated wavelet analysis carried out in this work has previously been presented in detail by Bloomfield *et al.* (2006). In the current study only the power outside the COI is retained.

To estimate the energy flux we made the assumption that all registered oscillations are acoustic. Therefore, the energy flux is estimated using the expression:

$$F_h = \rho_h v^2 c_h, \quad (3)$$

where,  $\rho_h$  is the density at the height  $h$ , and  $c_h$  the corresponding speed of sound. The values of  $\rho_h$  and  $c_h$  used in this work are presented in Table II.

To determine the velocity of the particles, two methods were used. Doppler velocities were obtained from the line bisectors with a method similar to the one used by Wunnenberg, Kneer and Hirzberger (2002) and they were used as representative of the velocity of the detected oscillations. This procedure is conducted over the whole data set regardless of the location of the detected oscillations. In the second method wavelet analysis was used. Wavelet analysis contains informations on both the amplitude and phase of the detected oscillations. The velocity amplitudes determined by the wavelets are used in Equation (3). The majority of the Doppler velocities shown in the velocity maps belong to non-oscillatory behavior. Only amplitudes which belong to the detected oscillations are taken into account here.

#### 4. Results

Our data show a wide range of oscillations. Figure 3 shows the oscillations with the largest amplitudes within the frequency range of 1mHz to 22mHz. The same range of frequencies were registered in both velocity and intensity.

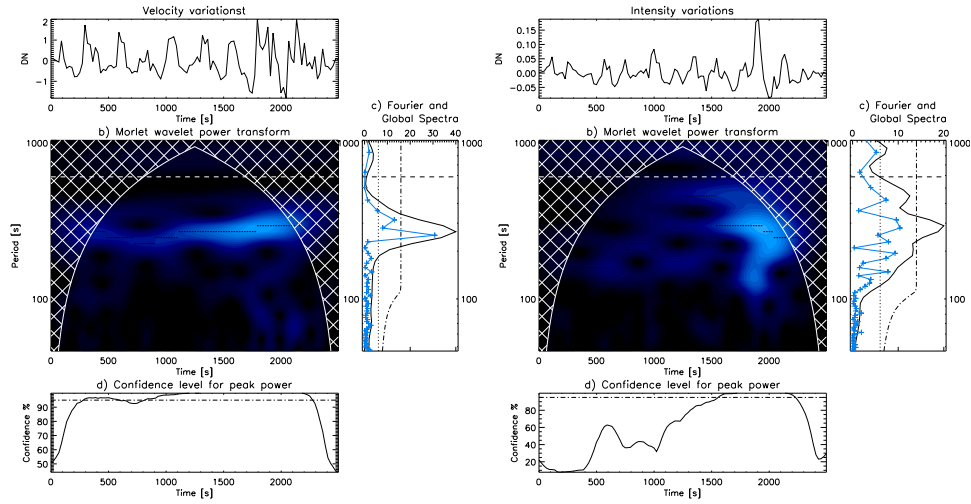


*Figure 3.* The oscillations with the largest amplitudes within the frequency range of 22mHz to 1mHz. The left panel shows the oscillations observed within the Doppler velocity temporal variation and the right panel oscillations observed within the intensity variation. Top panels marked with Velocity and Intensity variations present the actual signal which is submitted to the wavelet analysis. Below the result of the wavelet analysis is showed, marked with Morlet wavelet power transform, the registered power is presented in the color-coded-multilevel contours, where the minimum power corresponds to the black color and the maximum to the white. The dashed line on this presentation represent the maximum acceptable period detection. On the bottom of each wavelet presentation the confidence level for the peak power is presented and on the right side global and Fourier spectra are plotted for each signal, dash-dotted line in this diagram present the statistical significance of the registered power.

After an inspection by eye of light curve and cycle duration of the wave trains no direct evidence for a correlation in the two waveforms is found.

The duration of the oscillations is also analyzed. This parameter can be useful in interpreting the energy associated with a wave (Bloomfield *et al.* , 2006). The detections were sampled in terms of their duration with uniform full-cycle binning with a separate analysis been preformed in the velocity and intensity space.

Figure 4 shows the period distribution of the observed velocity and intensity oscillations as a function of the number of cycles. It is noticeable that not the same wave trains are observed. Also it is noticeable that most of the power for the velocity oscillations is contained within waves with duration of one cycle, while intensity oscillations last for a larger number of cycles.

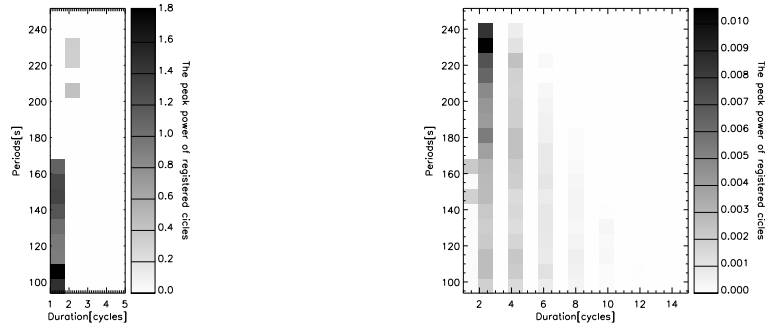


*Figure 4.* Period distribution of observed velocity ( left) and intensity ( right) oscillations (ordinate) as a function of duration of wavelet detection (abscissa). The various shades of gray represent the maximum power of the observed oscillation cycle in accordance with the scale shown. This image presents non-filtered data for the core of the observed spectral line.

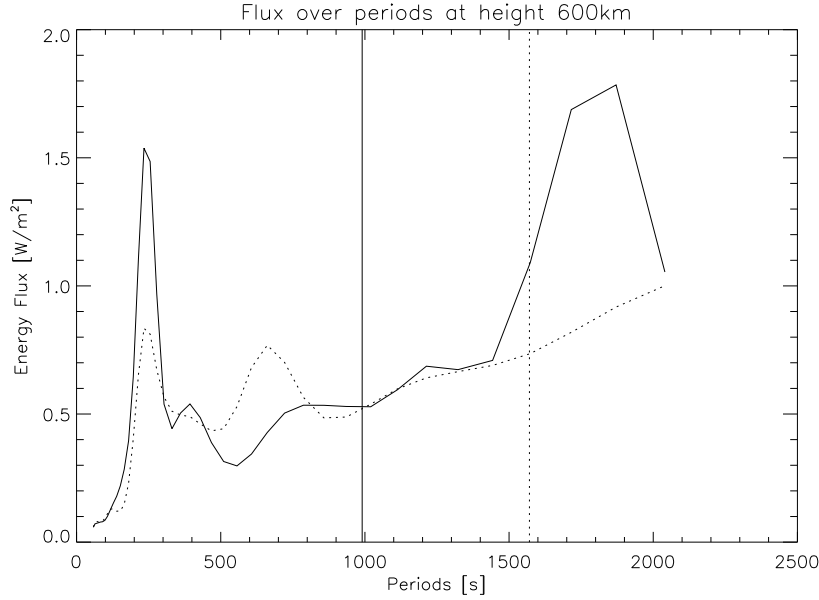
#### 4.1. ENERGY TRANSPORT AND THE DISSIPATION OF ENERGY

To investigate how much energy is carried by acoustic waves the LTE model (Holweger and Müller , 1974) was used to determine the density and corresponding speed of sound for heights used in the analysis. We have made the assumption that all registered power is acoustic. The velocity profiles, taken from wavelet analysis, are inserted into Equation (3), which provides an estimate of the energy flux. The calculated fluxes are presented in Figures 5 and 6.

An inspection of Figures 5 and 6 shows that the estimated flux is decreasing with period in both cases. The energy flux is larger at the lower atmospheric height. The energy flux estimates derived from the velocity maps (Figures 5 and 6) take into account that each pixel spends only a limited amount of time in oscillation. Therefore the average in this case is a reflection of the temporal behavior of the energy flux.

Data set DS4 has a cadence of 22.7s, making observations of high frequency waves possible. According to Ulmschneider (1971a, 1971b, 2003) there should be more energy flux detected when observations approach frequencies around 25mHz. A higher cadence should allow us to measure higher energy fluxes. Never the less, there is no significant increase in the estimated energy using DS4.

The first method for the estimating the particle velocity yields the results presented in TableIII. There is no significant difference with the energy flux estimated using the bisector method of Wunnenberg, Kneer and Hirzberger (2002) and wavelet method.



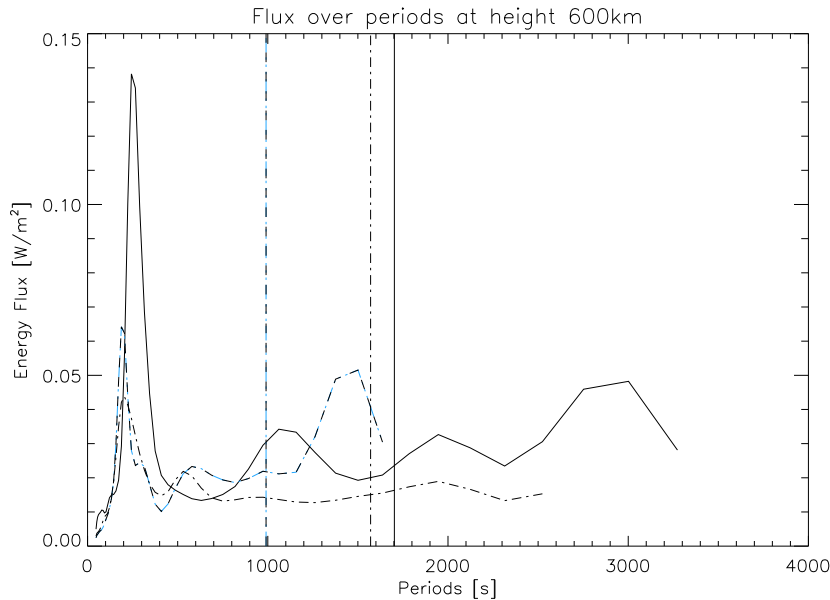
*Figure 5.* Estimated acoustic flux using velocity maps ( ordinate) as a function of periods of registered oscillations (abscissa) at the height of 300km. Solid lines represent results from the data set DS2. Dashed lines represent results from the data set DS1, while vertical lines represent the credible period.

Table III. Energy flux for the data sets DS6. The flux is calculated using the velocity averaged over the corresponding velocity maps of the data set.

data set	cadence [s]	$F_{660}$ [ $\text{W m}^{-2}$ ]	$F_{308}$ [ $\text{W m}^{-2}$ ]	$v_{660}$ [ $\text{W m}^{-2}$ ]	$v_{308}$ [ $\text{km s}^{-1}$ ]
DS1	28.4	0.005	0.103	0.57	0.42
DS2	28.4	0.003	0.064	0.32	0.26
DS3	28.3	0.045	N/A	0.62	N/A
DS4	22.7	0.005	N/A	0.62	N/A

## 5. Discussion and Conclusions

High frequency waves were detected at heights of 300 and 660km above the photosphere. The observations used in this work include internetwork, bright network with G-band structures and a pore. We find no evidence for a correlation between velocity and intensity oscillations. The estimated acoustic energy flux is found to be insufficient for heating the chromosphere.



*Figure 6.* Estimated acoustic flux using velocity maps (ordinate) as a function of periods of registered oscillations (abscissa) at the height of 660km. Solid lines represent results from the data set DS4. Dashed lines represent results from the data set DS2, blue dashed-dotted lines results from the data set DS3 and dashed-dotted line from the data set DS1. The vertical lines represent the credible period, where the style of the line correspond above assigned ones to the data sets.

When establishing possible errors in observing high frequency waves, the whole observations and data reduction procedures need to be considered. The influence of atmospheric seeing is mainly visible during speckle reconstruction. The work by von der Lhe (1984, 1993, and 1994) estimates an error of 10% in intensity introduced by speckle reconstruction. Of course, the most important part of reconstruction is the noise filtering. In this work we followed the recommendations of de Boer (1996), when setting the noise filter.

The seeing influence is most visible with differing data cadences. In the case of good seeing, cadence was lower (see Section 2) than in the case of very good and excellent seeing conditions. Therefore the amount of noise remaining after speckle reconstruction tended to vary only inside predicted error levels (von der Lhe, 1984, 1993, 1994; de Boer, 1996).

To make an estimate of the observed energy flux several assumptions were made. The first assumption was the use of the LTE model (Holweger and Mller, 1974). Since the core of the line used is in the non-LTE area,

being just above the temperature minimum (Vernazza, Avret and Loeser, 1981) and the strong lines of neutral iron do suffer from a non-LTE effect in both their opacity and in their source function (Shchukina, Trujillo Bueno and Kostik, 1997), future studies should include these effects.

Wunnenberg, Kneer and Hirzberger (2002) find no correlations between velocity and intensity oscillations and our findings agree with them. In our analysis the velocity oscillations tend to last for less cycles than the intensity oscillations.

Previous studies on this topic have also found a lack of sufficient energy flux from acoustic waves. The work by Schmieder and Mein (1980) found an energy flux of  $2 \text{ Wm}^{-2}$  over the frequency range 0mHz to 10mHz -the lower frequency range than the one presented here. The work by Schmieder and Mein (1980) was concentrated on the middle chromosphere, while here we study the upper photosphere and lower chromosphere. Also work by Lites and Chipman (1979) investigates the similar range of frequencies from 0mHz to 11.1mHz and state that the energy flux is too low to heat the chromosphere. The work by Mein and Mein (1976) observed high frequency waves in the range 10mHz to 15mHz at a height range of 800 to 1800km and also established that there is not enough energy present to heat the chromosphere. Liu (1974) observed the oscillations in the same frequency range and heights as the present work, but his estimated energy flux was several orders of magnitude higher than the energy fluxes found here. In light of the recent theoretical work (Kalkofen, 1990, 2001; Ulmschneider, 2003) the energy estimated in the work of Liu (1974) should be enough for heating the chromosphere. Wunnenberg, Kneer and Hirzberger (2002) reach the same conclusion. Our findings do not agree with them. One of the main differences between the work of Wunnenberg, Kneer and Hirzberger (2002) and the present study has to do with velocity response functions of the Fe I 543.45nm line. In this work, the velocity response functions were not used and only oscillations which are 99% significant were taken into account. The recent study by Fossum and Carlsson (2006) has also concluded that acoustic waves do not carry sufficient energy flux for the heating of the chromosphere.

The energy estimates on Figures 5 and 6 show a difference of one order of magnitude for the energy flux calculated for the spectral lines Fe I 543.45nm and Fe I 543.29nm. To get an estimate which reflect the temporal behavior for the corresponding data set only pixels which actually belong to the observed oscillation were taken into account. Since the majority of the observed oscillations were short lived we do not distinguish between waves of different duration. If we average over the whole time sequence, the observed oscillations cover 99% to 100% of the field of view for Fe I 543.45nm in DS1, DS2 and DS4. The corresponding coverage for Fe I 543.29nm is 72% to

81% in DS1 and DS2. Therefore the averaging for the energy estimates on Figures 5 and 6 is done for whole field of view.

One of the main assumptions used in the current and previous studies is that all registered oscillatory power is acoustic. This assumption is incorrect even for quiet internetwork regions. Domínguez (2003) found that the magnetic flux in the quiet internetwork is smeared by insufficient resolution and therefore underestimated. He also found that there are areas in the quiet internetwork which have magnetic fields comparable to those from the pores. Trujillo Bueno, Shuckina and Asensio Ramos (2004) claim that we can only see 1% of the magnetic field present in quiet internetwork regions. Andjic and Wiehr (2006) and Andic and Vočkić (2007) show evidence for some magnetic activity in quiet internetwork regions used in this work.

### Acknowledgements

I acknowledge the Ph.D. scholarship from Max Planck Institut for Solar System Research (Max Planck Institute für Sonnensystemforschung), Katlenburg-Lindau, Germany.

I wish, especially, to thank Dr. N. Shchukina for calculating the formation heights for the used lines.

During the work itself, I had lots of stimulating discussions for which I wish to thank R. Cameron, A. Vögler and E. Wiehr. I wish to thank P. Sutterlin and K. Janssen for giving me the software for the data reduction. For the help with the observations I wish to thank J. Hirzberger and K. Puschmann.

I also wish to thank M. Mathioudakis with help in formulating the sentences and together with D.B. Jess for help with the English.

### References

- Anderson, L.S., Athay, R.G. :1989, *Astrophys. J.* **336**, 1010  
 Andjic, A. :2006, *Serb. Astron. J.* **172**, 27  
 Andjic, A., Wiehr E. :2006, *Publ. Astron. Obs. Belgrade* **80**, 367  
 Andic, A., Vočkić, N. *Serb. Astron. J.*, submitted  
 Asplund, M., Nordlund, Ø.A., Trampedach, R., Allende Prieto, C., Stein, R.F. :2000, *Astron. Astrophys.* **359**, 729  
 Bendlin, C., Volkmer, R., Kneer, F. :1992, *Astron. Astrophys.* **257**, 817  
 Berkefeld, Th., Soltau, D. von der Lhe, O. :2003, *Proceedings of the SPIE* **4839**, 544  
 Bloomfield, D.S., McAteer, R.T.J., Mathioudakis, M., Keenan, F.P. :2006 *Astrophys. J.* **652**, 812  
 de Boer, C.R., Kneer, F., Nesis, A. :1992, *Astron. Astrophys.* **257**, L4  
 de Boer, C.R., Kneer, F. :1994, In Robertson, J.G., Tango, W.J. (eds.), *Very High Angular Resolution Imaging, IAU Symp.* **158**, 398

- de Boer,C.R. :1996, *Astron. Astrophys. Suppl.* **120**, 195  
 Carlsson,M., Stein,R.F. :1995 *Astrophys. J.* **440**, L29  
 Cram,L.E., Keil,S.L., Ulmschneider,P.:1979, *Astrophys. J.* **234**, 768  
 Deubner,F.L., Laufer,J. :1983, *Solar Phys.* **82**, 151  
 Dominguez,I.F. :2004, *Quiet Sun Magnetic Fields*, Copernikus GmbH, Katlenburg-Lindau, Germany, p.111  
 Durrant,C.T. :1980, *Astron. Astrophys.* **89**, 80  
 Fossum,A., Carlsson,M., :(2006), *Astrophys. J.* **646**, 579  
 Hansteen,V.H., Betta,R., Carlsson,M.: 2000, *Astron. Astrophys.* **360**, 742  
 Holweger,H., Müller,E.A.: 1974, *Solar Phys.* **39**, 19  
 Janssen,K.: 2003, *Struktur und Dynamik kleinskaliger Magnetfelder der Sonnenatmosphäre*, Copernikus GmbH, 2003, Kaltenburg-Lindau, Germany, p.123  
 Kalkofen,W.: 1990,In: Priest, E.R., Krishan, V. (eds.),*Basic Plasma Processes on the Sun,IAU Symp.* **142**, 197  
 Kalkofen,W.: 2001, *Astrophys. J.* **557**, 376  
 Keller,C.U., von der Lühe,O.: 1992, *Astron. Astrophys.* **261**, 321  
 Koschinsky,M., Kneer,F., Hirzberger,J. :2001, *Astron. Astrophys.* **365**, 588  
 Lighthill,M.J.: 1951, *Proceedings of the Royal Society A* **211**, 564  
 Lites,B.W., Chipman,E.G.: 1979, *Astrophys. J.* **231**, 570  
 Liu,S.Y. :1974, *Astrophys. J.* **189**, 359  
 Mein,N., Mein,P. :1976 *Solar Phys.* **49**, 231  
 Proudman,I. :1952*Proc. Roy. Soc. London A* **214**, 119  
 Schmieder,B., Mein,N. :1980, *Astron. Astrophys.* **84**, 99  
 Shchukina,N.G., Trujillo Bueno,J., Kostik,R.I.: 1997, *Solar Phys.* **172**, 117  
 Shchukina,N.G., Trujillo Bueno,J.: 2001, *Astrophys. J.* **550**, 970  
 Soltau D., Berkefeld,Th., von der Lühe,O., Wöger,F., Schelenz,Th. :2002, *Astron. Nachr.* **323**, 236  
 Stein,R.F.: 1967, *Solar Phys.* **2**, 385  
 Stein,R.F., Leibacher,J.: 1974, *Astron. Astrophys.* **12**, 407  
 Torrence,C., Compo,G.P.: 1998, *Bull. Amer. Meteor. Soc.* **79**, 61  
 Trujillo Bueno,J., Shchukina,N., Asensio Ramos,A.:2004, *Nature* **430**, 326  
 Ulmschneider,P.: 1971a, *Astron. Astrophys.* **12**, 297  
 Ulmschneider,P.: 1971b, *Astron. Astrophys.* **14**, 275  
 Ulmschneider,P.:2003 In: Antia, H.M., Bhatnagar, A., Ulmschneider,P. (eds.), *Lectures on solar Physic,Lecture Notes in Physics* Vol.619, Springer Verlag, Berlin, p.232  
 Vernazza,J.E., Avrett,E.H.,Loeser,R. :1981, *Astrophys. J.* **45**, 635  
 von der Lühe,O. :1984, *J.Opt.Soc.Am A* **1**, 510  
 von der Lühe,O. :1994a, *Astron. Astrophys.* **281**, 889  
 von der Lühe,O. :1994b, *Astron. Astrophys.* **268**, 347  
 von Uexküll,M., Kneer,F., Mattig,W., Nesis,A., Schmidt,W.: 1985, *Astron. Astrophys.* **146**, 192  
 Wunnenberg,M., Kneer,F., Hirzberger,J.: 2002, *Astron. Astrophys.* **395**, L51  
 Wunnenberg,M., Andjic,A., Kneer,F.: 2003,*Astron. Nachr.***324**, 356